Photoinitiated H-Atom Reactions in CO_2–HBr Complexes

Seung Koo Shin, Curt Wittig,*

Department of Chemistry, University of Southern California, Los Angeles, California 90089-0482

and William A. Goddard, III*

Materials and Molecular Simulation Center, Beckman Institute, 139-74, California Institute of Technology, Pasadena, California 91125 *(Received: March 8, 1991)*

Photoinitiated reactions of H atoms with CO_2 in CO_2–HBr complexes have been examined by using ab initio generalized valence bond–configuration interaction calculations. Recent experiments have shown that CO_2–HBr complexes yield OH ~40 times more efficiently than CO_2–HCl complexes for similar values of $h\nu - D_0(HX)$. We find that the calculated equilibrium geometry for the T-shaped CO_2–HBr complex is in excellent agreement with the experimental geometry, which is inertially asymmetric with the Br–C line almost perpendicular to the CO_2 axis and the H–Br bond nearly parallel to the CO_2 molecular axis. We find a linear isomer of CO_2–HBr to also be stable; this species has not been observed experimentally. We find that photoexcitation of the T-shaped HBr moiety leads to two directly dissociative excited states of A′ and A″ symmetries. For both states, the HBr bond expands rapidly following photoexcitation with most H atoms leaving unreactively from the complex. However, for those H atoms that approach CO_2 and form HOCO, the two excited states show dissimilar interactions due to interaction of the Br atom with HOCO. The A′ state has a weak in-plane bonding interaction between the Br p orbital and the C radical orbital of HOCO, whereas the A″ state leads to repulsion. These results are consistent with the experimental observations and underscore the greater variety possible in such relations taking place in complexes vs under single-collision, gas-phase conditions.

I. Introduction

Gas-phase chemical reaction dynamics depend strongly upon the relative orientations, alignments, and velocities of reactants, as well as their electronic configurations and orbital alignments.[1] These entrance-channel parameters determine reaction trajectories on the potential energy surface (PES) and influence overall cross sections, branching ratios, product state distributions, and reaction times. However, in most gaseous environments, there is no control over incident angles, impact parameters, and orbital alignments.

Attempts to control entrance-channel geometric properties have utilized interactions of the molecule with external electric or magnetic fields and have yielded exciting results for specific alignments and orientations.[2-13] In addition, alignment of reactant orbitals in chemical reactions has been achieved via the laboratory anisotropy of electronic excitation using polarized lasers.[14-17] We have employed a third strategy in achieving such orientation by utilizing the intermolecular interactions present in weakly bonded reaction-precursor complexes.[18-37] The anisotropic intermolecular force field responsible for binding the complex aligns precursor–molecular components regioselectively, leading to precursor–geometry-limited (PGL) reactions that offer a novel means of investigating regiospecific effects. In addition, photoinitiation provides control of the reaction energy by varying the photolysis wavelength, as well as "setting the clock" for the reaction by using ultrashort laser pulses.[38-40]

(1) Levine, R. D.; Bernstein, R. B. *Molecular Reaction Dynamics and Chemical Reactivity*; Oxford Press: New York, 1987.
(2) Kramer, K. H.; Bernstein, R. B. *J. Chem. Phys.* **1965**, *42*, 767.
(3) Beuhler, B. J.; Bernstein, R. B.; Kramer, K. H. *J. Am. Chem. Soc.* **1966**, *88*, 5332.
(4) Parker, D. H.; Chakravorty, K. K.; Bernstein, B. B. *J. Phys. Chem.* **1981**, *85*, 466.
(5) Gandhi, S. R.; Curtiss, T. J.; Xu, Q. X.; Choi, S. E.; Bernstein, R. B. *Chem. Phys. Lett.* **1986**, *132*, 6.
(6) Gandhi, S. R.; Xu, Q. X.; Curtiss, T. J.; Bernstein, R. B. *J. Phys. Chem.* **1987**, *91*, 5437.
(7) Brooks, P. R. *J. Chem. Phys.* **1969**, *50*, 5031.
(8) Marcelin, G.; Brooks, P. R. *J. Am. Chem. Soc.* **1975**, *97*, 1710.
(9) Brooks, P. R. *Science* **1976**, *193*, 11.
(10) van den Ende, D.; Stolte, S. *Chem. Phys. Lett.* **1980**, *76*, 13.
(11) Stolte, S. *Ber. Bunsenges. Phys. Chem.* **1982**, *86*, 413.
(12) Stolte, S. *Atomic and Molecular Beam Methods*; Scoles, G. Ed.; Oxford University Press: New York, 1987; Chapter 25.
(13) Parker, D.; Jalink, H.; Stolte, S. *J. Phys. Chem.* **1987**, *91*, 5427.
(14) Karney, Z.; Estler, R. C.; Zare, R. N. *J. Chem. Phys.* **1978**, *69*, 5199.
(15) Zare, R. N. *Ber. Bunsenges. Phys. Chem.* **1982**, *86*, 422.
(16) Rettner, C. T.; Zare, R. N. *J. Chem. Phys.* **1982**, *77*, 2416.
(17) Johnson, M. A.; Allison, J.; Zare, R. N. *J. Chem. Phys.* **1986**, *85*, 5723.
(18) Jouvet, C.; Soep, B. *Chem. Phys. Lett.* **1983**, *96*, 426.
(19) Breckenridge, W. H.; Jouvet, C.; Soep, B. *J. Chem. Phys.* **1986**, *84*, 1443.
(20) Zehnacker, A.; Duval, M. C.; Jouvet, C.; Lardeux-Dedonder, C.; Solgadi, D.; Soep, B.; Benoist-D'Azy, O. *J. Chem. Phys.* **1987**, *86*, 6565.
(21) Jouvet, C.; Duval, M. C.; Soep, B. *J. Phys. Chem.* **1987**, *91*, 5416.
(22) Duval, M. C.; Benoist-D'Azy, O.; Breckenridge, W. H.; Jouvet, C.; Soep, B. *J. Chem. Phys.* **1986**, *85*, 6324.
(23) Jouvet, C.; Duval, M. C.; Soep, B.; Breckenridge, C.; Whitham, C.; Visticot, J. P. *J. Chem. Soc., Faraday Trans.* **1989**, *85*, 1133.
(24) Keller A.; Visticot, J. P.; Tsuchiya, S.; Zwier, T. S.; Duval, M. C.; Jouvet, C.; Soep, B.; Whitham, C., unpublished work, 1990.
(25) Buelow, S.; Radhakrishnan, G.; Catanzarite, J.; Wittig, C. *J. Chem. Phys.* **1985**, *83*, 444.
(26) Radhakrishnan, G.; Buelow, S.; Wittig, C. *J. Chem. Phys.* **1986**, *84*, 727.
(27) Buelow, S.; Noble, M.; Radhakrishnan, G.; Reisler, H.; Wittig, C.; Hancock, G. *J. Phys. Chem.* **1986**, *90*, 1015.
(28) Buelow, S.; Radhakrishnan, G.; Wittig, C. *J. Phys. Chem.* **1987**, *91*, 5409.
(29) Häusler, D.; Rice, J.; Wittig, C. *J. Phys. Chem.* **1987**, *91*, 5413.
(30) Rice, J.; Hoffmann, G.; Wittig, C. *J. Chem. Phys.* **1988**, *88*, 2841.
(31) Wittig, C.; Sharpe, S.; Beaudet, R. A. *Acc. Chem. Res.* **1988**, *21*, 341.
(32) Wittig, C.; Engel, Y. M.; Levine, R. D. *Chem. Phys. Lett.* **1988**, *153*, 411.
(33) Chen, Y.; Hoffmann, G.; Oh, D.; Wittig, C. *Chem. Phys. Lett.* **1989**, *159*, 426.
(34) Wittig, C.; Hoffmann, G.; Chen, Y.; Iams, H.; Oh, D. *J. Chem. Soc., Faraday Trans. 2* **1989**, *85*, 1292.
(35) Hoffmann, G.; Oh, D.; Iams, H.; Wittig, C. *Chem. Phys. Lett.* **1989**, *155*, 356.
(36) Hoffmann, G.; Oh, D.; Wittig, C. *J. Chem. Soc., Faraday Trans.* **1989**, *85*, 1141.
(37) Shin, S. K.; Chen, Y.; Oh, D.; Wittig, C. *Philos. Trans. R. Soc. London A* **1990**, *332*, 361.
(38) Scherer, N. F.; Khundkar, L. R.; Bernstein, R. B.; Zewail, A. H. *J. Chem. Phys.* **1987**, *87*, 1451.

0022-3654/91/2095-8048$02.50/0

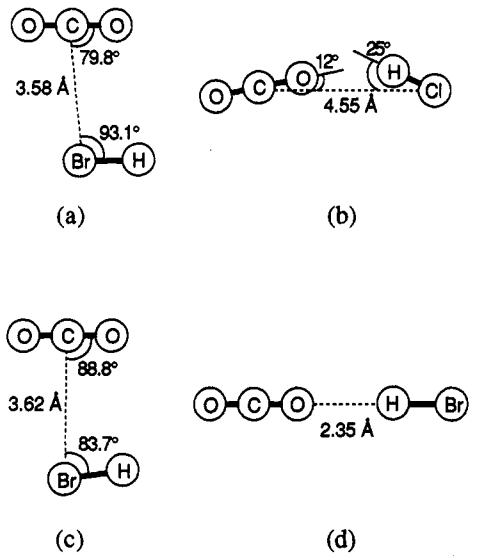

Figure 1. Experimental geometries (i.e., averaged over vibrational ground state) for (a) CO_2–HBr (refs 48 and 49) and (b) CO_2–HCl (refs 50 and 51). Theoretical geometries for (c) ground state T-shaped CO_2–HBr and (d) locally stable linear CO_2–HBr. Calculations were at the MP2 level, and counterpoise corrections were included.

The reaction of H atoms with CO_2 is endothermic by 25.5 kcal/mol and has been studied extensively under both bulk (i.e., single collision, arrested relaxation) and complexed conditions.[25,26,31,32,34,38-47]

$$H + CO_2 \rightarrow OH + CO \quad \Delta H_{298} = 8960\ cm^{-1} \qquad (1)$$

With complexes, relative reaction probabilities were obtained for CO_2–HBr and CO_2–HCl,[37] which have pronounced geometric differences, as shown in Figure 1. High-resolution infrared spectroscopic studies of these weakly bonded complexes in our laboratory[48,49] showed that CO_2–HBr is inertially asymmetric, with the Br–C line essentially perpendicular to the CO_2 axis, and the H–Br bond parallel on average to the CO_2 molecular axis, while CO_2–HCl is near-linear, with the hydrogen bonded to the oxygen.[50,51] These two regioselective precursors showed remarkably different reaction probabilities for the end-on (CO_2–HCl) and broadside (CO_2–HBr) geometries, the latter producing OH ~40 times more efficiently than the former.[37,52]

Figure 2 displays OH $A^2\Sigma \leftarrow X^2\Pi$ (0,0) LIF signals taken at the Q-branch bandhead $\{Q_{11}(7) + Q_{22}(2) + Q_{22}(3)\}$ for photoinitiated reactions in (i) CO_2–HBr complexes at 193 nm, (ii) CO_2–HBr complexes at 222 nm, (iii) CO_2–HCl complexes at 193 nm, and (iv) the corresponding bulk reactions. This enables a comparison to be made between relative reaction probabilities for end-on and broadside precursors.[37,52] With CO_2–HCl complexes, the reaction probability was so low that it was almost impossible

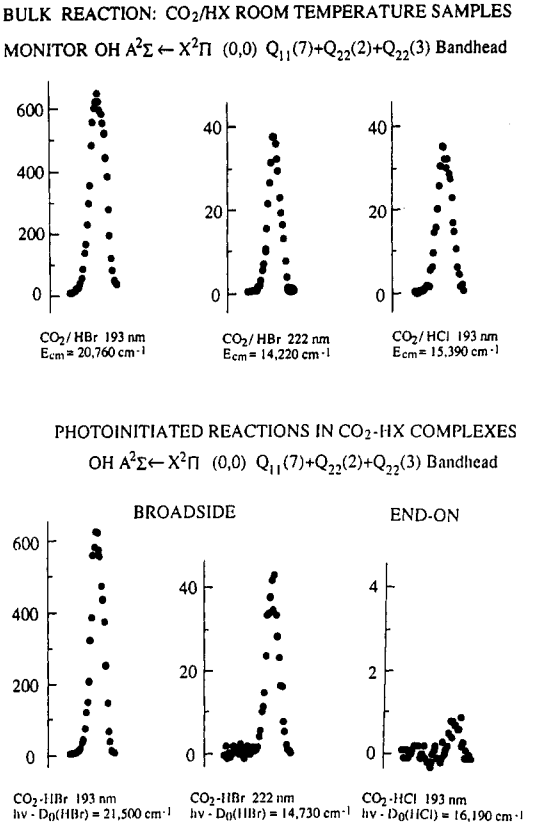

Figure 2. OH $A^2\Sigma \leftarrow X^2\Pi$ (0,0) LIF signals obtained at the Q branch bandhead $[Q_{11}(7) + Q_{22}(2) + Q_{22}(3)]$ for bulk conditions (upper entries) and for CO_2–HBr and CO_2–HCl complexes (lower entries). Typically, 20 shots per point were averaged for CO_2–HBr, while 200 shots per point were averaged for CO_2–HCl. Note the vertical scale changes (ref 37).

to get an OH LIF signal. After carrying out all normalizations (laser fluences, HX absorption coefficients, CO_2–HX concentrations), we deduced that *CO_2–HBr yields OH about 40 times more efficiently than CO_2–HCl.*[37,52] Values of $h\nu - D_0$ for 193-nm HCl and 222-nm HBr photolyses (16 100 and 14 800 cm^{-1}, respectively) are sufficiently close that the corresponding bulk reactions produce similar OH yields. Furthermore, measurements of the OH yield as a function of HI photolysis wavelength with CO_2–HI complexes showed a smooth monotonic variation and cannot be responsible for such a large difference.[33] Since the remaining difference between CO_2–HCl and CO_2–HBr complexes is geometrical, the observed difference was attributed to different reaction probabilities for end-on and broadside complexes, the latter being favored.[37,52]

Results obtained by using complexes differ from those obtained under bulk conditions and suggest the possibility that the complexes might involve two reactions leading to the same products. With CO_2–HBr complexes, nascent OH state distributons show less rotational excitation than with their bulk counterparts. From fitting the OH rotational distributions to a distribution of $HOCO^\dagger$ energies, we find a lowering of the energy in excess of reaction threshold, $E^\dagger$, by ~22% from the corresponding bulk value.[32] Moreover, with complexes, the distribution has a cold part, which might be due to additional mechanisms such as higher than binary complexes, exit-channel interactions, formation of Br–C(O)–OH, etc.[32] Deuterium substitution leaves the OH rotational energy distributions unaffected,[28] and sub-Doppler resolution measurements of average OH kinetic energies indicate that translational degrees of freedom are diminished slightly relative to bulk reactions.[34]

Time-resolved studies of OH production from CO_2–HI complexes using picosecond pump and probe pulses reveal that OH product accrues on a time scale of a few picoseconds, with the buildup time varying slightly with photolysis wavelength. OH buildup becomes increasingly rapid as the photolysis wavelength is decreased and can be fitted with a double-exponential rise,

(39) Scherer, N. F.; Sipes, R. B.; Bernstein, R. B.; Zewail, A. H. *J. Chem. Phys.* **1990**, *92*, 5239.
(40) Zewail, A. H. *Sci. Am.* **1990**, Dec. 76.
(41) Flynn, G. W.; Weston, R. E. *Annu. Rev. Phys. Chem.* **1986**, *37*, 551.
(42) Kleinermanns, K.; Wolfrum, J. *Laser Chem.* **1983**, *2*, 339.
(43) Kleinermanns, K.; Wolfrum, J. *Chem. Phys. Lett.* **1983**, *104*, 157.
(44) Kleinermanns, K.; Linnebach, E.; Wolfrum, J. *J. Phys. Chem.* **1985**, *89*, 2525.
(45) Quick, C. R.; Tiee, J. J. *Chem. Phys. Lett.* **1983**, *100*, 223.
(46) Schatz, G. C.; Fitzcharles, M. S.; Harding, L. B. *Faraday Discuss. Chem. Soc.* **1987**, *84*, 359.
(47) Schatz, G. C. Fitzcharles, M. S. In *Selectivity in Chemical* Reactions Whitehead, J. C., Ed.; Kluwer Academic Publishers: Dordrecht, 1988.
(48) Sharpe, S.; Zeng, Y. P.; Wittig, C.; Beaudet, R. A. *J. Chem. Phys.* **1990**, *92*, 943.
(49) Zeng, Y. P.; Sharpe, S.; Shin, S. K.; Wittig, C.; Beaudet, R. A. *J. Chem. Phys.*, in press.
(50) Altman, R. S.; Marshall, M. D.; Klempere, W. *J. Chem. Phys.* **1982**, *77*, 4344.
(51) Shea, J. A.; Read, W. G.; Campbell, E. J. *J. Chem. Phys.* **1983**, *79*, 614.
(52) Shin, S. K.; Chen, Y.; Nickolaisen, S.; Sharpe, S. W.; Beaudet, R. A.; Wittig, C. In *Advances in Photochemistry*; Volman, D., Hammond, G.; Neckers, D., Eds.; Wiley: New York, 1991; p 249.

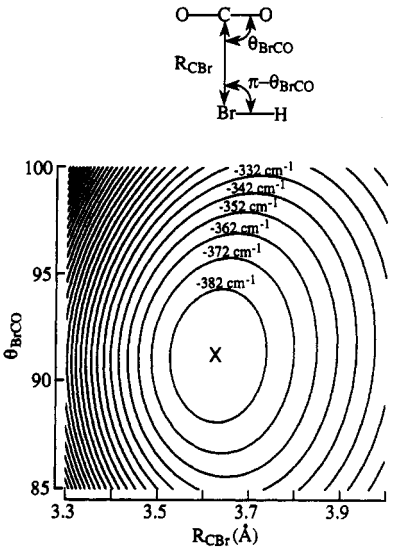

Figure 3. Potential contours for T-shaped CO_2–HBr as a function of R_{CBr} and Θ_{BrCO}. The HBr and OCO were kept parallel ($\Theta_{HBrC} = \pi - \Theta_{BrCO}$). Calculations were at the MP2 level and were corrected for BSSE. The minimum of −392 cm^{-1} is at R_{CBr} = 3.62 Å and Θ_{BrCO} = 88.8°.

although a single-exponential rise fits the data almost as well.[39]

In order to provide a better understanding of this complicated elementary chemical reaction, we carried out ab initio quantum chemistry calculations with extended basis sets. To determine geometries for the ground-state complexes, we used Møller–Plesset second-order perturbation (MP2) methods.[53] To calculate energies for a number of points in the ground and excited states, we used generalized valence bond (GVB)–configuration interaction (CI) methods.[54-56] These results indicate several important aspects of such photoinitiated reactions that may also apply to other systems.

II. Results and Discussion

A. Geometrical Properties. The calculated equilibrium geometry of the inertially T-shaped ground state is shown in Figure 1 along with the equilibrium geometry of the linear isomer. The MP2 energies were corrected for basis set superposition error (BSSE). Figure 3 shows the potential contours as a function of C–Br distance, R_{CBr}, and Br–C–O angle, Θ_{BrCO}, with HBr and OCO kept parallel ($\Theta_{HBrC} = \pi - \Theta_{BrCO}$). The minimum is at R_{CBr} = 3.62 Å and Θ_{BrCO} = 88.8°. The H atom lies in the Br–CO_2 plane, and Θ_{HBrC} = 83.7° is the optimized value at R_{CBr} = 3.62 Å and Θ_{BrCO} = 88.8°.

The dependence of the potential on orientation is shown in Figure 4 for both in-plane (Θ_{HBrC}) and out-of-plane (φ) changes (with Br and CO_2 kept at the equilibrium geometry). The twofold rotational barrier (184 cm^{-1}) for the out-of-plane H bend is lower than the rotational barriers (340 and 1250 cm^{-1}) for the in-plane H bend. [These barriers are for fixed R_{CBr} = 3.62 Å, so that they are upper bounds; in particular, the 1250-cm^{-1} barrier will be much lower.] The calculated R_{CBr} equilibrium distance of 3.62 Å is in excellent agreement with the experimental value of $\langle R_{CBr} \rangle$ = 3.58 Å, and the bond angles are in reasonable agreement with the experimental results depicted in Figure 1a.[49] Calculated rotational constants (equilibrium values) are A = 0.373 24, B = 0.045 21, and C = 0.040 33 cm^{-1}, while the experimental values (averaged over the ground vibrational state) are 0.386 74, 0.046 18, and 0.041 06 cm^{-1}, respectively.[49] Force constants obtained from curve fits to the potentials shown in Figures 3 and 4 yield vibrational frequencies of 42 cm^{-1} for the R_{CBr} stretch, 50 cm^{-1} for the lateral slipping vibration, 113 cm^{-1} for the Θ_{HBrC} bend, and 70 cm^{-1} for the φ torsion. This corresponds to expectation values of ~0.2 Å, 7°, 28°, and 26°, respectively, for the magnitudes of the corresponding zero-point displacements. The optimum linear structure is strictly linear, with a hydrogen–oxygen bond distance of 2.35 Å. The binding energy (D_e) of the ground-state T-shaped complex is 392 cm^{-1} at the MP2 level, while that for the linear structure is 517 cm^{-1}. We expect a significant barrier between these isomers so that both should be observable. However, only the T-shaped isomer has been observed experimentally, i.e., from a high-resolution rovibrational absorption spectrum recorded by exciting the CO_2 asymmetric stretch vibration with a tunable diode laser.[49]

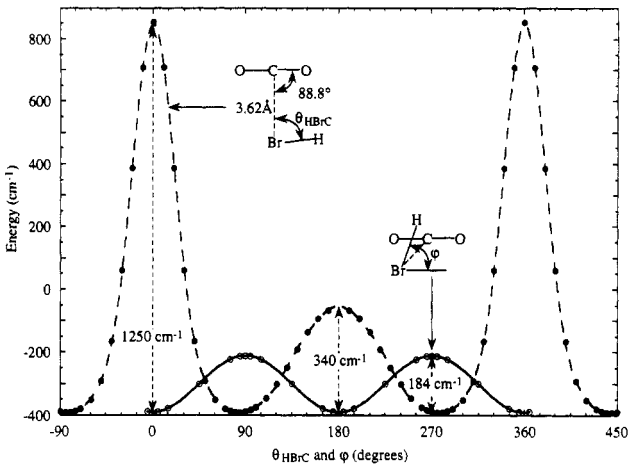

Figure 4. Potential curves as a function of Θ_{BrCO} (in-plane) and φ (out-of-plane) for the T-shaped CO_2–HBr complex (MP2 level with BSSE corrections). We kept R_{CBr} = 3.62 Å and Θ_{BrCO} = 88.8° for both curves. For out-of-plane φ, we also kept Θ_{HBrC} = 83.7°.

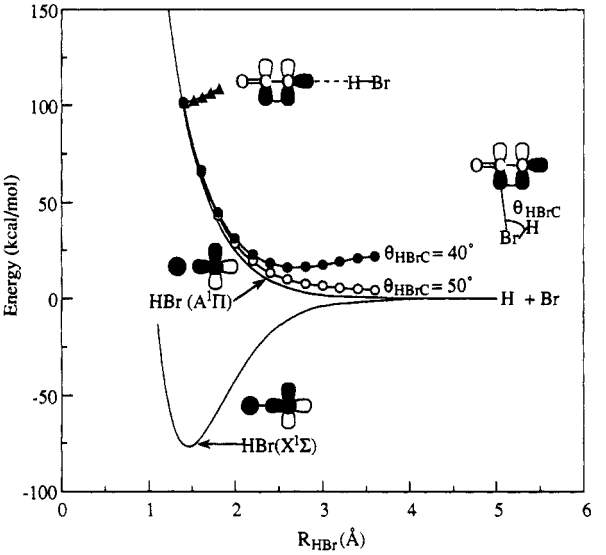

Figure 5. Potential curves (from GVB-RCI) for end-on and broadside approaches of hydrogen (Θ_{HBrC} = 40° and 50°) as well as the ground ($^1\Sigma$) and excited ($^1\Pi$) states of free HBr.

B. End-on vs Broadside Chemistry. In order to better understand the marked difference between end-on and broadside reaction probabilities,[37] total electronic energies were calculated for various pathways of H-atom movement by using the GVB-RCI method (described more completely in section IV). Since HBr photolysis involves electronic excitation from a nonbonding Br p_π orbital to the HBr σ^* orbital, photoinitiation prepares two near-degenerate excited states of A′ and A″ symmetries for the broadside case (i.e., in-plane and out-of-plane nonbonding bromine p_π orbitals, respectively), but leads to a degenerate excited Π state for the end-on case. With the broadside precursor at the

(53) *Gaussian 90*: Frisch, M. J.; Head-Gordon, M.; Trucks, G. W.; Foresman, J. B.; Schlegel, H. B.; Raghavachari, K.; Robb, M. A.; Binkley, J. S.; Gonzalez, C.; Defrees, D. J.; Fox, D. J.; Whiteside, R. A.; Seeger, R.; Melius, C. F.; Baker, J.; Martin, R. L.; Kahn, L. R.; Stewart, J. J. P.; Topiol, S.; Pople, J. A. Gaussian, Inc., Pittsburgh, PA, 1990.

(54) Goddard, W. A., III *Science* **1985**, *227*, 917.

(55) Carter, E. A.; Goddard, W. A., III *J. Chem. Phys.* **1988**, *88*, 3132.

(56) (a) Shin, S. K.; Beauchamp, J. L.; Goddard, W. A., III *J. Phys. Chem.* **1990**, *94*, 6963. (b) Shin, S. K.; Beauchamp, J. L.; Goddard, W. A., III *J. Chem. Phys.* **1990**, *93*, 4986.

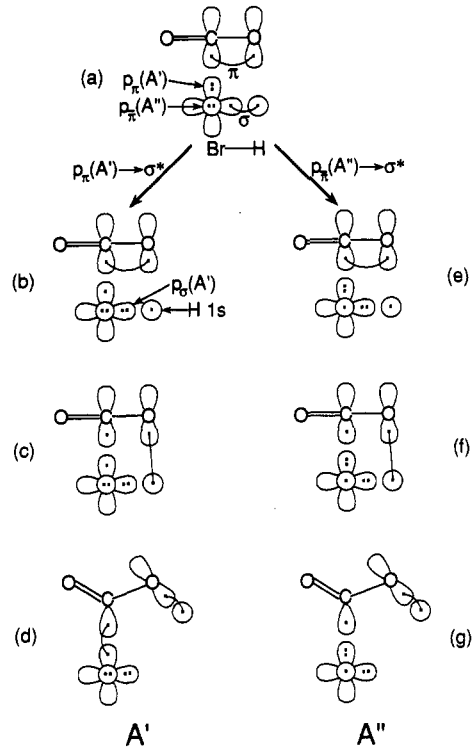

Figure 6. The valence bond electron correlation diagram for photoexcitation of the CO_2–HBr complex to form Br–C(O)–OH: (a) the VB description of the ground-state CO_2–HBr complex, (b) and (e) the excited-state CO_2–HBr complexes, (c) and (f) the hydrogen attack of an oxygen p orbital, (d) Br–C(O)–OH, and (g) Br + HOCO.

ground-state equilibrium geometry, the A″ state is lower in energy than the A′ state by ~0.5 kcal/mol. Figure 5 shows potentials for the end-on and broadside cases as a function of R_{HBr}; also included are calculated curves for the HBr $^1\Sigma$ ground and $^1\Pi$ excited states. The HBr $^1\Pi$ excited state is quite repulsive, dissociating to ground-state H + Br. Spin–orbit coupling is not considered. In excited CO_2–HBr broadside complexes, the variation of the potential with R_{HBr} is initially close to that of free HBr, while for end-on complexes, the H-atom approach toward oxygen is repulsive, as shown in Figure 5. This indicates that the end-on case is disfavored due to the repulsive nature of the hydrogen approach toward an oxygen nonbonding σ orbital. It also implies that the H atom in the linear precursor cannot acquire significant kinetic energy, except by being deflected from the linear path. On the other hand, HBr dissociation in the broadside precursor is *relatively* well developed before the hydrogen "attacks" the oxygen. Broadside H-atom approaches with Θ_{HBrC} values of 40° and 50° are shown in Figure 5. Thus it is quite reasonable that the broadside configuration is favored.

C. The Valence Bond Correlation Diagrams for Broadside Reactions. The valence bond (VB) correlation diagrams for evolution of two excited states in the broadside case are shown pictorially in Figure 6. Figure 6a shows the six relevant orbitals for the CO_2–HBr complex: the in-plane CO π bond (two orbitals), the Br nonbonding $p_\pi(A')$ and $p_\pi(A'')$ orbitals (two orbitals), and the HBr σ bond (two orbitals). Since HBr photolysis involves electronic excitation from a nonbonding p_π orbital to the σ* orbital, there are two near-degenerate excited states of A′ and A″ symmetries involving in-plane p_π and out-of-plane p_π nonbonding Br orbitals, respectively. Upon electronic excitation, the HBr σ and σ* orbitals evolve to a Br nonbonding $p_\sigma(A')$ orbital and a hydrogen 1s orbital as depicted in Figure 6, b and e, for A′ and A″ states, respectively. This hydrogen 1s orbital can couple with an oxygen p orbital of the in-plane CO π bonding orbital to form HOCO. This results in the release of a carbon radical orbital of HOCO as shown in Figure 6, c and f. For the A′ excitation, the bonding interaction between a carbon radical orbital of HOCO and the Br $p_\pi(A')$ orbital leads to the A′ ground state of Br–C(O)–OH. On the other hand, the A″ state leads to three-electron

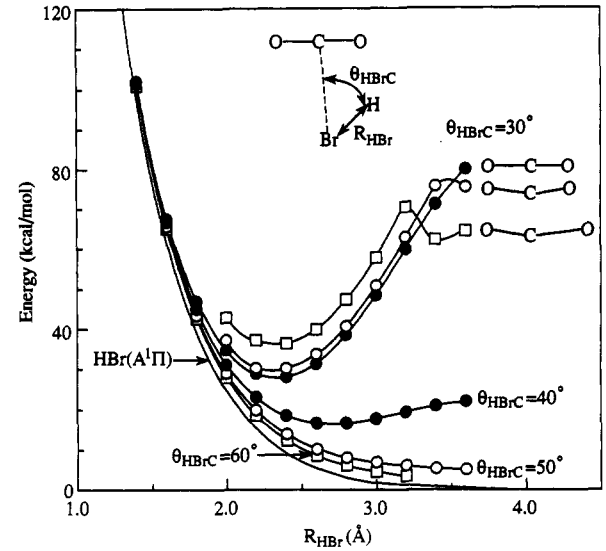

Figure 7. Energies of A′ and A″ excited states of the CO_2–HBr complex as a function of R_{HBr} and for various values of Θ_{HBrC}. For Θ_{HBrC} = 30°, the open circles and boxes correspond to distortions which indicate that CO_2 vibrational excitation promotes reactivity.

interactions in the C–Br bond region and correlates to the A″ excited state of Br–C(O)–OH.

D. Role of the Br–C(O)–OH Intermediate. The VB correlation diagram suggests for A′ the possible participation of the π–σ orbital switching product, Br–C(O)–OH, along the reaction pathway. This intermediate formation is analogous to the reverse process of the thermally activated σ–π orbital switching reaction of vicinal HX elimination from CH_3CH_2X.[57-60] With A″ excitation, there is a repulsive interaction between the doubly occupied Br p orbital aligned along the C–Br axis and the singly occupied carbon radical orbital of HOCO. However, with A′ excitation, Br can participate in the reaction in two ways. First, the singly occupied Br orbital along the C–Br axis can bind with the carbon p orbital of the in-plane CO π bond, releasing the in-plane oxygen p orbital which can in turn capture the incoming hydrogen. This activation process results in early formation of Br–C(O)–OH. Second, Br can wait until hydrogen attack of the oxygen releases the in-plane carbon p orbital to attract the singly occupied Br orbital. This capture process results in late formation of Br–C(O)–OH.

Using the GVB-RCI method, we examined the above interactions leading to the potential curves for both excited states of the CO_2-HBr complex, as shown in Figure 7. Since H-atom motion is fast relative to Br and CO_2 motions, the Br and CO_2 positions were frozen at the ground-state equilibrium geometry and the H atom was brought toward the oxygen. For hydrogen attack angles with Θ_{HBrC} greater than ~50°, HBr dissociation in the excited complex is close to that of free HBr, leading to unreactive trajectories. This suggests that the early bromine-carbon interaction is too weak to influence the reaction pathway. For Θ_{HBrC} = 40°, the potential curve becomes repulsive at R_{HBr} ~2.7 Å. For Θ_{HBrC} = 30°, the hydrogen approach becomes rapidly repulsive past R_{HBr} ~ 2.35 Å. The minimum corresponds to R_{HO} ~ 1.84 Å and Θ_{HOC} ~ 95.5°. The kinetic energy of hydrogen at this minimum is ~27% less than that from free HBr dissociation and may help explain why the experiments find that most of the OH product corresponds to a lowering of $E^\dagger$ of HOCO† by ~20% from its bulk value.[32] Such angles of reactive hydrogen approach can result from large-amplitude hydrogen motion in the plane. The calculated expectation value of the magnitude of the zero-point displacement for this motion is 28° and corresponds to Θ_{HBrC} = 56°. For an oscillator wave function

(57) Goddard, W. A., III *J. Am. Chem. Soc.* **1970**, *92*, 7520.
(58) Miller, S. I. *Adv. Phys. Org. Chem.* **1968**, *6*, 185.
(59) Benson, S. W.; Bose, A. N. *J. Chem. Phys.* **1963**, *39*, 3463.
(60) Benson, S. W.; Haugen, G. R. *J. Am. Chem. Soc.* **1965**, *87*, 4036.

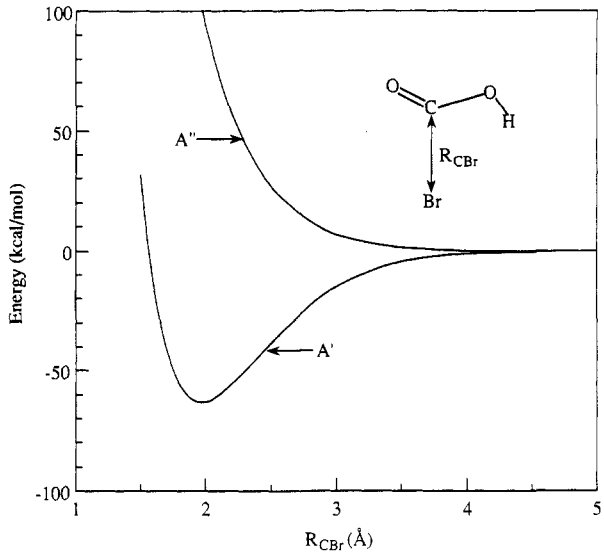

Figure 8. Potential curves calculated for the interaction between Br and HOCO in A′ and A″ states of Br–C(O)–OH as a function of R_{CBr} (GVB-RCI without BSSE corrections).

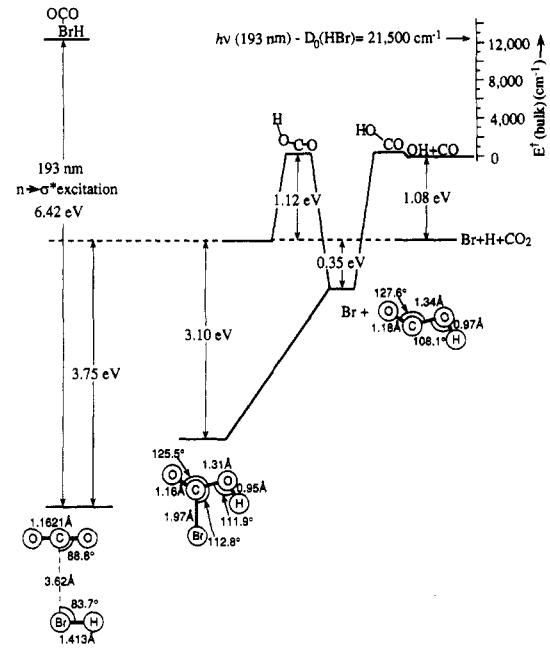

Figure 9. Energy diagram showing relevant stationary points.

that is near-Gaussian, there is significant probability of finding the hydrogen with $\Theta_{HBrC} \leq 50°$. Also, even though hydrogen excursion is limited by the binding energy of the complex, coupling with the other large-amplitude motions may further open reactive channels.

Figure 7 also shows the potential surface for $\Theta_{HBrC} = 30°$ with deformed CO_2 (to simulate the effect of vibrations due to the collisional impact). With CO_2 bent by an amount corresponding to the zero-point displacement, $V(R_{HBr})$ is higher at low values of R_{HBr} than the case of equilibrium CO_2. However, this reverses for $R_{HBr} > 3.4$ Å. With combined displacements (corresponding to the average zero-point displacements for the symmetric stretch, antisymmetric stretch, and bending vibrations), $V(R_{HBr})$ is higher than for the other two curves, but drops significantly from $R_{HBr} > 3.2$ Å. The increases in energy upon distortion for $R_{HBr} = 2$–3 Å are attributed to the CO_2 vibrational potential, while past ~3 Å, it is clear that the distortion facilitates reaction. This result suggests that vibrational excitation of CO_2 enhances the reaction probability by decreasing an entrance-channel dynamical barrier for the reaction.

The reaction of the photodissociated H with CO_2 should have a barrier analogous to that for the bulk reaction. This view is in accord with our observation of similar OH yield spectra (i.e., OH product vs. HI photolysis wavelength) from CO_2–HI complexes and bulk reactions.[33] For example, if the shape of the yield spectrum is determined by overcoming a dynamical barrier in broadside collisions, then it is reasonable that the curves are similar. Once hydrogen is captured by CO_2, forming $HOCO^\dagger$, the two excited states (A′ and A″) can follow dissimilar reaction pathways. In the A″ state, the interaction between Br and the singly occupied carbon orbital of HOCO is repulsive, as shown in Figure 8. Therefore, reaction on the A″ surface is expected to be similar in the exit channel to the bulk reaction. The difference between the complex and bulk reaction is in the entrance channel and may be due to underdeveloped HBr dissociation in the complex, as shown in Figure 7. However, in the A′ state, Br and HOCO can attract each other, forming a short-lived Br–C(O)–OH intermediate, as shown in Figure 8. In this process, decomposition of the Br–C(O)–OH intermediate into Br + HOCO is expected to result in recoil between the Br atom and HOCO. This results in less energy available for $HOCO^\dagger$ internal excitation than the bulk counterpart, in which there is no such complication caused by a nearby bromine atom. This may help explain, at least in part, the cold part of the OH rotational distribution, which corresponds to a lowering of $E^\dagger$ of $HOCO^\dagger$ to ~80% of its bulk value.[32] An overall potential energy diagram of this complicated photoinitiated reaction of hydrogen atom with CO_2 in the C-O_2–HBr complex is illustrated in Figure 9. The ground state of the Br–C(O)–OH intermediate lies ~15 kcal/mol above the ground state of the CO_2–HBr complex, and the C–Br bond energy (D_e) is 63.4 kcal/mol. The possible formation of Br–C(O)–OH has a significant implication in time domain spectra. Formation of this transient intermediate might slow OH formation, causing the OH production rate to deviate from the HOCO unimolecular decomposition rate. Also, direct observation of the OH rise time using CO_2–HI complexes suggests a possible double-exponential rise of the OH concentration,[39] which is consistent with the formation of a transient I–C(O)–OH intermediate.

III. Summary

We have employed ab initio GVB–CI methods to examine photoinitiated reactions of H atoms with CO_2 in CO_2–HBr complexes. The equilibrium geometry of the T-shaped ground-state complex is in excellent agreement with the experimental result. It is inertially asymmetric with the Br–C line almost perpendicular to the CO_2 axis and the H–Br bond nearly parallel to the CO_2 molecular axis. The linear isomer which has not been observed experimentally appears to be as stable as the T-shaped complex. The H atom in the T-shaped complex undergoes large-amplitude bending in the Br–CO_2 plane, i.e., an expectation value of 28° (half-angle) for the magnitude of the zero-point Θ_{HBrC} displacement. The Θ_{HBrC} angle of H-atom approach toward oxygen plays a major role in determining reactivity, and large-amplitude Θ_{HBrC} bend can accommodate a significant percentage of reactive events.

Photoexcitation of the HBr moiety prepares two excited-state CO_2–HBr complexes of A′ and A″ symmetries. In the entrance channel, where the approach angle of the H atom toward the oxygen is important, there is nothing to suggest different reaction probabilities for the two excited states, since the Br–C interaction is weak. This means that the entrance channel for the complex reaction is similar to broadside H + CO_2 bulk reactions, except that H–Br dissociation is not completely developed with the complex when the H atom confronts the entrance-channel barrier. Once the H atom attacks CO_2 and forms HOCO, however, the interaction between the Br atom and HOCO is important in determining the reaction pathway. Since the A′ and A″ state complexes correlate to the A′ ground and A″ excited states of the π–σ orbital switching product Br–C(O)–OH, respectively, this interaction is attractive in the A′ complex and would lead to formation of the Br–C(O)–OH intermediate, while this interaction is repulsive in reactions on the A″ surface. Therefore, photoinitiated reactions on the A″ surface are considered to be reactions of H atoms with CO_2 without participation of the Br atom during the course of the reaction, while reactions on the A′ surface may

TABLE I: Total Energies (hartrees) and Binding Energies (cm^{-1}) for Linear and T-Shaped CO_2–HBr Complexes and Their Subsystems;[a] In Both Cases, the Geometry Was Optimized at the MP2 Level (with the Double-ζ plus Double-Polarization Basis Set)

	level			
molecule	HF	ΔE^b	MP2	ΔE^b
linear				
CO_2–HBr	−201.208 684	−223 (−321)	−201.839 283	−517 (−860)
CO_2(HBr)	−187.683 412		−188.172 874	
HBr(CO_2)	−13.524 257		−13.664 055	
T-shaped				
CO_2–HBr	−201.208 082	−56 (−189)	−201.838 479	−392 (−683)
CO_2(HBr)	−187.683 272		−188.172 392	
HBr(CO_2)	−13.524 553		−13.664 300	
free				
CO_2	−187.683 021		−188.171 811	
HBr	−13.524 201		−13.663 554	

[a] All geometries are given in Figure 1 and section IVB. Here, CO_2(HBr) represents CO_2 molecule with basis sets for HBr but without any potentials for HBr. [b] $\Delta E = E(CO_2\text{–HBr}) - E[CO_2(HBr)] - E[CO_2(HBr)]$ is in units of cm^{-1}, and binding energies in parentheses are with basis set superposition errors.

involve later stage formation of the π–σ orbital switching intermediate Br–C(O)–OH. This model accommodates the various experimental findings about similarities and differences between the bulk and complexed reactions, such as (i) the relatively cold OH rotational state distribution under complexed conditions, (ii) the somewhat slower OH rise time observed with the CO_2–HI complexes than would be expected from simply HOCO unimolecular decomposition, and (iii) differences in reactivities for end-on and broadside precursors. Furthermore experimental identification of the transient formation of X–C(O)–OH under matrix-isolated conditions as well as theoretical (both ab initio molecular orbital and dynamical) investigations of this reaction on the full potential surface would provide valuable information about this elementary photoinitiated reaction of H atoms with CO_2 in weakly bonded CO_2–HX complexes.

IV. Computational Details

A. Basis Sets. We employed valence double-ζ basis sets for carbon (9s5p/3s2p) and oxygen (9s5p/3s2p),[61] augmented with one set of d-polarization functions for carbon and oxygen [ζ^d(C) = 0.73 and ζ^d(O) = 1.07] optimized for CO_2 at the GVB(4/8) level. Unscaled valence double-ζ basis sets[61] were used for hydrogen (4s/2s) augmented with one set of p-functions (ζ^p = 0.6). Double-ζ basis sets for bromine (3s/3p/2s2p) with effective core potentials[62] were used with one set of d-polarization functions (ζ^d = 0.45) optimized for HBr at the GVB(1/2) level and augmented with one set of diffuse d-functions (ζ^d = 0.15). The present basis sets for the hydrogen and bromine yield a HBr bond dissociation energy of D_e = 87.3 kcal/mol at the GVB(1/2) dissociation-consistent CI level, which is comparable to the experimental value of D_e = 90.1 kcal/mol.[63] The estimated dipole moment using charge populations obtained from the Mulliken population analysis is 0.78 D which is comparable to the experiment (0.79 D).[64]

TABLE II: Optimum Geometries for the T-Shaped Complex at Various Calculational Levels

parameter	HF[a]	HF-CP[b]	MP2[a]	MP2-CP[b]
R_{CBr}, Å	3.89	4.00	3.46	3.62
Θ_{BrCO}, deg	87.4	87.2	89.4	88.8
Θ_{HBrC},[c] deg	92.1	94.0	62.2	83.7

[a] Without basis set superposition error corrections. [b] With basis set superposition error corrections by using the counterpoise (CP) method. [c] The R_{CBr} and Θ_{BrCO} were kept at 3.62 Å and 88.8°.

B. Geometries. Experimental geometries of CO_2(R_{CO} = 1.1621 Å)[65] and HBr (R_{HBr} = 1.413 Å)[63] were used, and the equilibrium geometries of CO_2–HBr complexes were determined at the MP2 level with extended basis sets augmented with one set of diffuse functions for carbon, oxygen, and hydrogen (ζ^d(C) = 0.17, ζ^d(O) = 0.287, and ζ^p(H) = 0.2). Basis set superposition error (BSSE) was accounted for by using the counterpoise method.[66] Table I summarizes total energies of the linear and T-shaped CO_2–HBr complexes and their subsystems. Table II summarizes the calculated geometry for the T-shaped complex at various theoretical levels. HOCO geometries were taken from SDCI calculations using polarized valence double-ζ basis sets by Schatz et al.[46] The ground-state geometry of Br–C(O)–OH was optimized at the HF level by using a gradient optimization program.[67]

C. Theoretical Method. With GVB-RCI, we start with the GVB-PP wave function in which the four CO_2 bond pairs and the one HBr bond pair are correlated at the perfect pairing level [GVB(5/10)]. The RCI (restricted CI) includes all configurations in which the two electrons of each correlated pair are allowed to have all three possible occupations among the two natural orbitals.[53-56] Thus, for five pairs, there are 3^5 = 243 spatial configurations and 654 spin eigenfunctions. The RCI lifts the spin-coupling restriction of GVB-PP and also allows interpair correlation (ionic configuration) in which movement of charge in one bond pair is correlated with simultaneous movement of charge in an adjacent bond pair. The RCI wave function generally provides a reasonable description of potential curves for most reactions by allowing for optimization of spin coupling and by including the dominant interpair and intrapair correlations.[53,68]

Acknowledgment. This research was supported by National Science Foundation Grants CHE88-22067 (C.W.) and CHE83-18041 (W.A.G.), and by the U.S. Army Research Office under the auspices of the Center for the Study of Fast Transient Processes.

Registry No. CO_2, 124-38-9; HBr, 10035-10-6; H_2, 1333-74-0; OH•, 3352-57-6.

(61) Dunning, T. H.; Hay, P. J. *Methods of Electronic Structure Theory*; Schaefer, H. F., III. Ed.; Plenum: New York, 1977; Chapter 1.
(62) Wadt, W. R.; Hay, P. J. *J. Chem. Phys.* **1985**, *82*, 284.
(63) Herzberg, G. *Spectra of Diatomic Molecules*; Van Nostrand Reinhold: New York, 1950.
(64) Townes, C. H.; Schawlow, A. L. *Microwave Spectroscopy*; Dover: New York, 1975.
(65) Herzberg, G. *Electronic Spectra and Electronic Structure of Polyatomic Molecules*; Van Nostrand Reinhold; New York, 1966.
(66) Boys, S. F.; Bernardi, F. *Mol. Phys.* **1970**, *19*, 553.
(67) Rappe', A. K.; Bierwagen, E. P.; Goddard, W. A., III, unpublished work.
(68) Harding, J. B.; Goddard, W. A., III *J Am. Chem. Soc.* **1975**, *97*, 6293.